Title: Prevalence of multiple subtypes of binocularly-modulated visual neurons in the mouse superior colliculus

Running Title: Binocular neurons in mouse SC

Authors: Ashley L. Russell, PhD[1] and Jason W. Triplett, PhD[1,2]

Author affiliations: [1]Center for Neuroscience Research, Children's National Hospital, Washington DC and [2]Departments of Pediatrics and Pharmacology & Physiology, The George Washington University School of Medicine and Health Sciences, Washington, DC

Author profile: Ashley Russell obtained her MS from the University of Buffalo and PhD from Uniformed Services University before moving on to work as a Postdoctoral Research Fellow at Children's National Hospital. She completed the work for this manuscript during her postdoctoral training where she employed anatomical and physiological techniques to understand visual system processing and circuit development.

Keywords: vision, binocular, subcortical, circuit

Key points summary

- Binocular integration of input from both eyes is necessary for complex visual processing.
- Recent evidence demonstrated that binocular integration occurs in retinorecipient sub-cortical structures, in addition to cortical regions.

- The superior colliculus (SC) is well-positioned to be involved in binocular integration due to its input from the ipsilateral and contralateral eyes, however there is no functional evidence of binocular neurons in the mouse SC.
- Using *in vivo* electrophysiology, we showed that there is a high prevalence of binocular neurons in the mouse anteromedial SC and these are similar to, but distinct from the neighboring monocular neurons.

Funding

This work was supported by NIH R01 EY025627 (JWT), NIH R21 EY029874 (JWT), and the District of Columbia Intellectual and Developmental Disabilities Research Center (DC-IDDRC) Award U54HD090257 by NICHD (PI: V. Gallo).

Acknowledgements

We thank members of the Triplett and Corbin labs for helpful discussions and critical reading of the manuscript.

Abstract

A central role of the visual system is to integrate inputs from both eyes to form one coherent visual perception. The superior colliculus (SC) plays a central role in visual processing, gaze orientation and vergence eye movements necessary for binocular vision. Indeed, the SC receives direct inputs from both the contralateral and ipsilateral eye and binocularly-modulated neurons have been identified in the SC of multiple species. However, evidence for binocular processing in rodents, particularly mice, has not been functionally confirmed. In this study we recorded visually-evoked activity in the mouse SC while presenting visual stimuli to each eye individually or both together and reveal a surprising diversity of binocularly-modulated responses. Strikingly, we found that ~2/3 of all identified neurons in the anteromedial SC were binocularly-modulated. Furthermore, we identified four binocular subtypes based on their differential responses under varying ocularities of stimulus presentation. Interestingly, we found both orientation- and direction- selective (OS and DS, respectively) neurons in all four binocular subtypes. And, tuning properties of binocular neurons were distinct from neighboring monocular neurons, exhibiting more linear spatial summation. Together, these data suggest that binocular neurons are prevalent in the anteromedial SC of the mouse. Additionally, the distinct tuning properties of binocular neurons suggest a previously unappreciated complexity of visual processing in the SC, which may contribute to binocular perception.

Introduction

Integration of visual information from both eyes allows for complex visual perceptions, such as disparity selectivity and stereopsis. While the traditional dogma has been that binocular integration occurs exclusively in cortical structures such as the primary visual cortex (V1) (Scholl, Burge et al. 2013, Zhao, Liu et al. 2013), recent evidence has emerged demonstrating that binocular integration may occur in subcortical image-forming structures as well. Indeed, studies in the dorsal lateral geniculate nucleus (dLGN) of the thalamus in multiple species have revealed previously unappreciated binocular interactions (Grieve 2005, Howarth, Walmsley et al. 2014, Zeater, Cheong et al. 2015). Remarkably, these circuits even display ocular dominance and orientation-matching plasticity akin to that observed in V1 (Gu and Cang 2016, Jaepel, Hubener et al. 2017, Huh, Abdelaal et al. 2020), suggesting subcortical nuclei could serve as useful models for understanding principles of binocular circuit development, organization, and function.

The superior colliculus (SC) is another image-forming retinorecipient nucleus that receives visual input and regulates critical head and eye movements (Basso and May 2017). Intriguingly, the SC participates in vergence eye movements necessary for binocular vision, suggesting a central role in detecting and responding to binocular visual stimuli (Chaturvedi and van Gisbergen 1999, Chaturvedi and Van Gisbergen 2000, Suzuki, Suzuki et al. 2004, Van Horn, Waitzman et al. 2013). Indeed, binocularly-modulated neurons have been identified in the SC of non-rodent species including opossum (Dias, Rocha-Miranda et al. 1991), cat (Berman, Blakemore et al. 1975, Mimeault, Paquet et al. 2004) and monkey (Goldberg and Wurtz 1972). However, their

prevalence in rodent species is not well understood. Initial studies in the mouse and hamster identified scant cells driven ipsilaterally or binocularly (Drager and Hubel 1975, Chalupa and Rhoades 1977). Of note, concurrent studies reported a substantial portion of binocular neurons in the anterior SC of the hamster (Tiao and Blakemore 1976).

The mouse SC has recently emerged as an attractive model to interrogate visual circuitry, where molecular and genetic tools can be leveraged (Ito, Feldheim et al. 2017). The mouse SC receives projections from 85-90% of retinal ganglion cells (RGCs), including those from both the contralateral and ipsilateral eyes (Ellis, Gauvain et al. 2016). And, investigations of the tuning properties of visual neurons in the SC have revealed intriguing sub-nuclear organizations (Ahmadlou and Heimel 2015, Feinberg and Meister 2015, Inayat, Barchini et al. 2015). A recent studied noted distinct preferences for direction of movement in the rostral SC between neighboring monocular and binocular zones (de Malmazet, Kuhn et al. 2018). However, the prevalence of binocular interactions and the tuning of putative binocularly-modulated (BN) neurons in the mouse SC remains unclear.

Here, we utilized *in vivo* electrophysiological recordings in anesthetized mice to characterize the responses of neurons in the anteromedial portion of the SC, where ipsilateral and contralateral RGC terminals are present, to visual stimuli presented to each eye individually or both together. Intriguingly, we found that about two-thirds of all identified neurons exhibited BN responses. Of these, four binocular subtypes could be distinguished based on their differential responses to varying ocularities of stimulation. As a group, binocular neurons in the SC were less selective for orientation of stimulus than their monocularly-driven neighbors, though orientation-selective (OS) units were

identified in three binocular subtypes. Intriguingly, binocular OS units exhibited linear spatial summation, in contrast to non-linear monocular neurons in the anteromedial SC found here or generally throughout the SC, as reported elsewhere (Wang, Sarnaik et al. 2010, Kay and Triplett 2017). Neither binocular nor monocular neurons in our dataset exhibited substantial selectivity for direction of movement; however, direction-selective (DS) units were identified in all four binocular subtypes. Taken together, these data demonstrate that BN neurons are prevalent in the mouse SC and are comprised of multiple subtypes, suggesting a complex contribution to visual processing in the SC and, potentially, downstream functionality necessary for binocular perception.

Methods

Ethical approval

All the experimental procedures, care and handling of animals were conducted in accordance with and approved by the Institutional Animal Care and Use Committee at Children's National Hospital.

Subjects

Adult (45-120 days of age) male and female C57BL/6J mice (RRID: IMSR_JAX:000664, Jackson Laboratory) were used for this study. Mice were bred and maintained in-house and the offspring were used in this study. After weaning, mice were same sex housed in groups of one to five per cage. Mice were housed in a temperature- (18-23 °C), humidity- (40-60%) and light-controlled (12 light/12 dark) room. Access to food and water was *ad libitum*.

In vivo electrophysiology

In vivo electrophysiological recordings were performed as previously described (Kay and Triplett 2017, Kay, Gabreski et al. 2018). Mice were anesthetized with isoflurane. A precision vaporizer (VetFlo, Kent Scientific) maintained isoflurane flow at 3.5-4.0% for induction and 0.75-1.25% for maintenance in 1 L/min oxygen flow. Ophthalmic ointment was placed on both eyes to prevent drying. After loss of reflexes, animals were placed on the recording platform where body temperature was maintained at 36-37 °C through a feedback-controlled heating pad monitored via a rectal thermoprobe (Stoelting). The skull was exposed, and connective tissue was removed to ensure adherence of the headplate. A custom-made Acrylonitrile Butadiene Styrene plastic headplate was tightly secured to the skull using superglue and dental cement. A craniotomy was performed on the right hemisphere, ~1.5-2.0 mm lateral from the midline and ~1.5 mm anterior from lambda using a branchpoint of the anterior cerebral artery as a reference to target the anteromedial region of the SC. Ophthalmic ointment was then fully removed from both eyes. A thin layer of silicone oil was then applied to the eyes to prevent drying while allowing for clear optical transmission.

A 16-channel silicone probe (NeuroNexus Technologies) was lowered between 1.0 and 1.6 mm into the SC at a 45° angle to the horizontal and ~45° angle to the midline. A polytrode electrode with 2 columns of sites (8 sites per column) at 50 μm intervals (model A1-16-Poly2-5mm-50s-177-A16) was used to sample a large space while allowing multiple representations across sites (Figure 1B). The shanks of the probes were 5 mm long, with a maximum width at the top of the shank of 68 μm. Probes

were coated in 1,1'-Dioctadecyl-3,3,3',3'-Tetramethylindocarbocyanine Percholate (DiI, Invitrogen) for post-procedure visualization of probe placement (Figure 1B). Electrical signals were amplified and filtered between 0.7 and 7 kHz, sampled at ~25 kHz and acquired using a System 3 workstation (Tucker-Davis Technologies). Signals were analyzed with custom software in MATLAB (MathWorks) and individual units were identified by spike sorting methods using independent components analysis, as previously described (Niell and Stryker 2008).

At the end of the recording, the animal was deeply anesthetized and intracardially perfused with ice-cold phosphate buffered saline (PBS) followed by 4% paraformaldehyde in PBS. Brains were sagittally sectioned at 150 μm with a VT1000 vibratome (Leica) and imaged on a BX63 Automatic Fluorescent Microscope (Olympus) for probe placement verification.

Visual stimuli

Visual stimuli were generated using custom MATLAB software, as previously described (Niell and Stryker 2008). The monitor (52 x 29.5 cm, 60 Hz refresh rate, ~35-45 cd/m^2 mean luminance) was placed 30 cm from the eyes, subtending ~80° x 50° of visual space and centered on the midline of the animal to maximize coverage of the binocular visual field. (Figure 1A). Visual stimuli consisted of drifting square waves (100% contrast) at 12 different orientations (30° spacing), six different spatial frequencies (between 0.01 and 0.32 cycles/º [cpd] over six logarithmic steps), and one temporal frequency (2 Hz) presented for 1.5 s with an inter-stimulus interval of 0.5 s (Figure 1A). In addition, full-field flash (0 cpd) and blank (gray) screens were presented to provide a

robust visual stimulus and determine spontaneous firing rate, respectively. Each stimulus condition was presented in 5-7 trials in a pseudorandom order in three different ocularity conditions: 1) binocularly to both eyes (BO), 2) monocularly to the eye contralateral to the recording site (CO), and 3) monocularly to the ipsilateral eye (IO) (Figure 1C). For monocular conditions, an opaque piece of cardboard was placed directly in front of the opposite eye to occlude it from viewing the screen. Following this, animals were again presented to the visual stimuli in the BO condition to ensure no confounding effect of anesthetic.

Visual tuning analysis

For each identified unit, we determined if the unit was visually responsive under each ocularity condition. To do so, we first determined the stimulus that elicited the highest mean firing rate in each ocularity condition. Since we and others have found that spontaneous rates of neurons in the SC are usually low (Wang, Sarnaik et al. 2010, Kay and Triplett 2017), we chose a stringent cutoff to determine if a unit was visually responsive. A unit was determined to be visually responsive if 1) the mean firing rate elicited by this stimulus was greater than 3 standard deviations above or below the spontaneous rate of the unit, 2) the firing rate elicited by this stimulus was greater than 3 standard deviations above or below the spontaneous rate in at least two-thirds of the trials, and 3) the mean firing rate was significantly different from the spontaneous rate based on a Wilcoxon's Rank Sum statistical test. Since we presented stimuli in the BO ocularity condition twice, we chose the epoch in which the sum of the mean rates across all visual stimuli was highest for further analysis. After determining visual

responsiveness under each ocularity condition, units were classified based on their responses (Figure 1D).

For visually responsive units, we further calculated the degree of orientation and directional tuning. To quantify the degree of orientation and direction selectivity, the global orientation and direction selectivity indices were calculated (gOSI and gDSI, respectively) (Inayat, Barchini et al. 2015, Shi, Barchini et al. 2017). gOSI and gDSI were calculated as the vector sum of responses normalized by the scalar sum of responses. gOSI was calculated as: $\frac{\sum R_\theta e^{i2\theta}}{\sum R_\theta}$, where R_θ is the mean firing rate at θ direction of gratings. gDSI was calculated as: $\frac{\sum R_\theta e^{i\theta}}{\sum R^\theta}$. A cell was considered orientation selective (OS) if it had a gOSI greater than 0.25 and a gDSI less than 0.25, while a cell was considered direction selective (DS) if it had a gDSI greater than 0.25. For OS and DS units, we determined the preferred spatial frequency as that which had the highest mean rate across all directions shown and the preferred direction after fitting the tuning curve with a wrapped gaussian to firing rates at each direction presented at the preferred spatial frequency (Niell and Stryker 2008). From this, we determined the preferred orientation for OS units by first normalizing the preferred direction to half of the full phase, i.e. 0° to 180°, then subtracting 90° to determine the orthogonal (Wang, Sarnaik et al. 2010). In addition, we determined the tuning width as the half-width at half-maximum of the fitted curve above the baseline and the F_1/F_0 ratio as the firing rate at the stimulus frequency divided by the mean rate.

Statistical Analysis

Statistical analysis was conducted on N=21 male and female animals. There was no difference between male and female responses. Each animal had one to nine visually responsive units, totaling N=93 neurons for analysis. All values are reported as mean ± standard deviation (SD). All data was tested for normal distribution using the Anderson-Darling test and outliers were identified using ROUT (GraphPad Software). In almost all cases, data was not normally distributed except for gOSI comparisons between monocularly-modulated (MN) and binocularly-modulated (BN) groups. For this comparison an unpaired t-test was used. For all MN versus BN comparisons in which the data was not normally distributed, data was analyzed using a Mann-Whitney test. Distributions between the neuronal subtypes were analyzed using the Kruskal-Wallis or Kolmogorov-Smirnov test. An $\alpha = 0.05$ was considered statistically significant. All analyses and graph plotting were done with Prism (GraphPad Software).

Results

Putative monocular and binocular neuronal subtypes in the anteromedial SC

To determine eye-specific influence on visual responsiveness in the anteromedial SC, drifting square waves were presented directly in front of the animal (Figure 1A) while a 16-channel silicone probe was placed in the anteromedial SC (Figure 1B). Animals were then exposed to 5-7 trials of stimuli in 3 different ocularity conditions: 1) both eyes open (BO) 2) only the contralateral eye to the recording site open (CO) or 3) only the ipsilateral eye open (IO) (Figure 1C). Units were considered visually responsive under a given ocularity condition if 1) the peak mean firing rate across all stimulus conditions shown was >3 SDs above the spontaneous rate, 2) this was the case in at

least two-thirds of the trials for the peak condition, and 3) the peak rate was significantly different from the spontaneous rate.

Using this method, we reasoned that 7 putative cells types could be encountered based on their response profile under each ocularity condition (Figure 1D). First, we defined monocularly-modulated (MN) units as those that were responsive in the BO condition and either the CO or the IO condition, but not all three. Such a response profile would indicate that the respective monocular condition (CO or IO) is driving the binocular response, thus leading to two distinct MN subtypes: contra-driven (MN-C) and ipsi-driven (MN-I). Next, we posited that putative binocularly-modulated (BN) units could have five potential response profiles. The first we term Simple (BN-S), wherein visual responses were elicited in all three BO, CO and IO ocularity conditions. The next we term Emergent (BN-E), which are visually responsive only when stimuli are presented in the BO condition, but not CO nor IO. Then, there is the possibility that a unit could respond in either the CO or IO condition, but not both nor when stimuli are presented binocularly. We term these units Inhibited by Ipsi (BN-IbI) and Inhibited by Contra (BN-IbC), since responses would only be observed when the ipsilateral or contralateral eye were occluded, respectively. A final possible profile we could observe would be a response when each eye is open individually, but not in the BO condition, which we term Cross-Inhibited (BN-CI).

Monocularly-driven units in the anteromedial mouse SC

Inputs from the retina are segregated into eye-specific layers in the anteromedial SC. Based on this and previous reports of visually responsive SC neurons (Wang,

Sarnaik et al. 2010, Ahmadlou and Heimel 2015), we expected to encounter a substantial number of units driven by monocular input from either eye. Indeed, we identified several MN-C units that were strongly responsive in both the BO and CO ocularity conditions (Figure 2A & B). However, peak rates in the BO condition tended to be higher than those in the CO condition (Figure 2C). In addition, we encountered a few units that appeared to be driven predominantly by inputs from the ipsilateral eye (Figure 2D & E). Consistent with previous data (Tiao and Blakemore 1976), these units tended to be weakly responding in the IO ocularity condition, though they did pass our relatively stringent criteria for visual responsiveness. In support of this, peak firing rates in the BO condition tended to be substantially higher than those observed in the IO condition for these units (Figure 2F). Taken together, these data suggest that monocularly-driven units are present in the anteromedial SC of the mouse, and these are predominantly driven by contralateral input.

Binocularly-modulated units in the anteromedial mouse SC

Though units responsive to inputs from both eyes have been described in the SCs of multiple species (Goldberg and Wurtz 1972, Berman, Blakemore et al. 1975, Dias, Rocha-Miranda et al. 1991), little support for their presence in the mouse SC has been put forth. In this study, however, we encountered four of the five putative types of BN subtypes could be identified (Figure 1D). First, we were able to identify several BN-S units that responded in all three ocularity conditions (Figure 3A & B). Next, the most prevalent type of BN units we encountered were BN-E, which were visually-responsive only when stimulus was presented to both eyes (Figure 3C & D). We also found a

handful of BN-IbI and BN-IbC units (Figure 3E-H), which responded only in the CO and IO conditions, respectively. However, among all visually responsive units analyzed; none met the criteria for BN-CI.

Overall, we found that BN cells comprise a large portion of cells in the anteromedial SC. Of the 93 cells we isolated, 31.18% are MN and 68.82% were BN (Figure 4A). As expected, the majority of MN cells were MN-C (86.21%) while only a small subset were MN-I (13.79%). In the BN group, isolated cells in each subtype made up the following proportions in the population: BN-S (15.63%), BN-E (65.63%), BN-IbI (7.81%) and BN-IbC (10.94%) (Figure 4A). There were no significant differences in baseline and peak firing rates when comparing MN and BN cell groups (Figure 4B). Additionally, there were no differences in baseline or peak firing rates amongst the subtypes (Figure 4C). However, in all comparisons, the peak firing rate was significantly higher than the baseline firing rate (Figure 4B and 4C). Together, these data suggest that both MN- and BN-modulated neurons are present in the anteromedial SC of the mouse, with MN-C and BN-E subtypes being the most prevalent.

Orientation selectivity of monocular and binocular subtypes in the anteromedial SC

We next sought to understand visual tuning of MN- and BN-modulated neuronal subtypes to the drifting square wave stimulus. Square waves were presented in 12 different orientations and 6 different spatial frequencies which allowed for analysis of orientation- and direction-selectivity between subtypes. Overall, there was no difference in mean gOSI between MN and BN groups (Figure 5A) nor between individual subtypes (Figure 5B). Interestingly, however, MN neurons had a larger percentage of visually

responsive units that were OS compared to BN neurons (82.76% vs 53.13%; Figure 5C). This shift in decreased percentage of OS BN units was apparent in most subtypes with the exception of BN-S units (Figure 5D). Of the MN subtypes, 84% of MN-C and 75% of MN-I neurons were OS. Of the BN cell subtypes, 80% of BN-S, 50% of BN-E, 40% of BN-IbI and 42.86% of BN-IbC neurons were OS (Figure 5D).

In subtypes in which visual responsiveness was observed in multiple ocularity conditions (i.e. MN-C, MN-I, and BN-S), we wanted to determine if orientation-selectivity was correlated across stimulus paradigms. There was a significant correlation between the gOSI calculated in CO and BO for MN-C units (Figure 5E), suggesting that selectivity is consistent across conditions. In contrast, we did not find a strong correlation between gOSI in BO and IO conditions for MN-I units (Figure 5F). However, this may be due to the low number of MN-I units we encountered. For BN-S units, there was a strong correlation in gOSI between BO and CO conditions (Figure 5G), which was less robust when comparing BO and IO conditions (Figure 5H). Taken together, these data suggest that a substantial proportion of both MN and BN visually responsive units in the anteromedial SC are tuned to oriented stimuli.

Subtype-specific tuning properties of OS neurons

Given that many visually responsive neurons were OS, we next examined tuning properties of this population of cells in both MN and BN subtypes. Based on our comparisons of gOSI between ocularity conditions, we first wanted to visualize tuning profiles under each condition. Representative polar plots of tuning responses of OS neurons for each identified subtype are presented in Figure 6A-F. Anecdotally, the plots

for MN-C, MN-I, and BN-S units appeared similar in the appropriate ocularity conditions (Figure 6A-C). To further investigate this, we determined the difference in preferred orientation under relevant conditions for these subtypes, defined as the minimum of the difference or its complement angle (Figure 6G). We found a significant effect of group and significantly increased differences in preferred orientation for BN-S units when comparing the difference found between BO and IO, as well as the difference found between CO and IO to the difference in preferred orientation found between BO and CO for MN-C units. These data, in combination with the reduced correlation between gOSI in BO and IO conditions for BN-S units, suggest that orientation-selectivity of these units may be predominantly dictated by contralateral rather than ipsilateral inputs. In addition, we found a trend towards an increase in the difference of preferred direction for MN-I units in comparison to MN-C units, again consistent with the lack of correlation in gOSI between BO and IO conditions we observed for MN-I units.

We next evaluated the distribution of preferred orientations for each subtype to determine if there were biases (Figure 6H). While we did not observe any significant differences in distributions between subtypes many of the preferred directions seemed to predominantly be clustered between -90° and -30°. Indeed, a comparison of the cumulative distribution of all OS units, regardless of subtype, was significantly different from a random distribution. And, the distributions of MN-C, BN-S, and BN-E were also significantly different than a random distribution. These data suggest that OS neurons in the anteromedial SC tend to prefer orientations ranging from vertical (-90/+90°) to obliquely angled leftward (-30°), regardless of MN or BN subtype.

Next, we examined the sharpness of tuning of OS units towards their preferred direction by calculating the tuning width of a best fit curve (Figure 6I). In general, OS neurons of all subtypes were sharply tuned, with mean tuning widths ranging from 21.8° to 41.9°. Despite this wide range, we did not find a main effect of subtype nor any differences between individual subtypes.

In addition to examining preference for direction/orientation, we also evaluated tuning for varying spatial frequencies of OS units. Across subtypes, we observed OS units exhibited preference for the full range of spatial frequencies tested. Indeed, we found no difference in preference for different spatial frequencies (Figure 7A). We also examined the sharpness of spatial frequency tuning by calculating the bandwidth of a best-fit curve. For most subtypes, OS units were broadly tuned to spatial frequency, with bandwidths ranging up to three octaves. While MN-I units tended to be more sharply tuned for spatial frequency, we did not observe a significant effect of subtype (Figure 7B). Lastly, we wondered if spatial frequency preference might vary between ocularities for those subtypes that responded under multiple conditions. Interestingly, while most MN-C, MN-I and BN-S OS units exhibited the same spatial frequency preference across ocularity conditions, we did observe substantial differences in some cases (Figure 7C). Intriguingly, shifts in preference went in both directions, sometimes being higher under BO condition and sometimes lower. We did not observe differences in the mean change in spatial frequency preference across subtypes.

Finally, we determined the linearity of spatial summation for MN- and BN-modulated subtypes by calculating the F_1/F_0 ratio of OS neurons (Skottun, De Valois et al. 1991). Typically, a value greater than 1 is considered linear, while a value less than 1

is considered non-linear spatial summation. Consistent with previous reports (Wang, Sarnaik et al. 2010, Kay and Triplett 2017), most units in the anteromedial SC were non-linear. Intriguingly, BN units had a higher mean F_1/F_0 ratio, although this was not significant (Figure 8A). This trend was more apparent when examining individual subtypes (Figure 8B); for instance, 50% of BN-IbI and all BN-IbC units identified were linear (Figure 8C). However, we did not detect an effect of subtype on mean F_1/F_0 ratio. We next asked whether linearity varied between ocularity conditions for MN-C, MN-I and BN-S subtypes. Intriguingly, the mean difference in F_1/F_0 ratio was at or below zero for each comparison, suggesting that response is less linear (<1.0) in the BO condition in comparison to single eye conditions (Figure 8D). However, we found no effect of subtype on shift in F_1/F_0. Altogether, these data suggest that BN cells, specifically BN-IbI and BN-IbC, may have more linear spatial summation of stimuli in the visual field than other subtypes.

Increased direction-selectivity in binocularly-modulated subtypes

Finally, we sought to determine direction-selectivity in MN and BN cell subtypes. In general, the majority of cells were OS, however, we also isolated several DS units. Intriguingly, the majority of the DS units we identified were BN-modulated. Indeed, none of the MN units we isolated passed our threshold for direction-selectivity (gDSI of 0.25), while 10.16% of BN units did (data not shown). Further, we found a significant increase in mean gDSI in BN cells compared to MN cells (Figure 9A). Interestingly, at least one unit of all four BN-modulated subtypes we identified in the anteromedial SC was DS (Figure 9B-F). However, a one-way ANOVA comparing gDSI between subtypes

revealed no significant difference (Figure 9B). Importantly, the proportions of DS neurons we encountered were substantially lower than previous reports of overall rates of direction-selectivity in the SC (Wang, Sarnaik et al. 2010, Kay, Gabreski et al. 2018). Interestingly, the single BN-S DS unit we identified showed varying levels of direction-selectivity depending on ocularity condition (BO: 0.31, CO: 0.22, IO: 0.08), suggesting the interaction between contra- and ipsi-RGC inputs plays an important role in shaping selectivity. Despite this, the preferred directions of this unit were closely related across ocularity conditions (BO: 26.3, CO: 32.0, IO: 37.4) (Figure 9C). Taken together, these data suggest that BN-modulated neurons tend to be more DS than MN-modulated neurons in the anteromedial SC, and all subtypes of BN-modulated neurons can exhibit selectivity for direction of movement.

Discussion

The SC is a midbrain structure that receives visual information and regulates orienting movements, including vergence eye movements required for binocular vision. However, the tuning properties of binocular neurons in the SC are not well understood, especially in rodents. Here, we characterized the modulation of visual responses by binocular inputs in the mouse SC, focusing on the anteromedial region. In contrast to previous studies, we identified a substantial number of BN neurons, which could be segregated into four functional subtypes based on their differential responses to stimuli presented monocularly or binocularly. While the proportion of BN neurons classified as OS was reduced compared to neighboring MN cells, all four BN subtypes exhibited orientation-selectivity to some degree. Furthermore, evidence of direction-selectivity

was also exhibited by all four BN subtype populations. Together, these data suggest that binocular interactions in the mouse SC are more common than previously assumed and that BN neurons exhibit a variety of tuning properties.

Prevalence of BN neurons in the mouse SC

While previous studies of visual tuning properties in the rodent SC suggested that minimal binocular interactions or even ipsilaterally-influenced responses were observed in the SC (Drager and Hubel 1975, Chalupa and Rhoades 1977), we found a surprising proportion of the units we identified in the anteromedial mouse SC were BN. Indeed, BN neurons comprise over half (68.82%) of the units, despite relatively stringent criteria for visual responsiveness. The lack of evidence for binocularity in the rodent SC in previous studies could be driven by experimental methods or analysis strategies or a combination of both.

First, while the mouse SC receives bilateral input from both contralateral and ipsilateral RGCs, the contralateral RGC input to the SC is dense while the ipsilateral input is sparse. Previous studies have shown that contralateral terminals assume a volume of ~401×10^{-6} mm^3 while ipsilateral terminals only assume 9.83×10^{-6} mm^3 (Haustead, Lukehurst et al. 2008). And, these inputs are segregated into distinct laminae in the SC. Eye-specific segregation itself does not preclude binocularity, as has been demonstrated in the dLGN (Grieve 2005, Howarth, Walmsley et al. 2014, Zeater, Cheong et al. 2015). But, the organization of ipsilateral terminals in the mouse dLGN may lend itself to easier identification of binocular neurons. In the mouse, ipsilateral RGC terminals are clustered in the center of the bean-shaped dLGN and surrounded on

all sides by contralateral RGCs. Combined with the convoluted, interwoven nature of dendritic and axonal terminals (Morgan, Berger et al. 2016), provides ample opportunity for convergence of inputs from both eyes. Indeed, recent trans-synaptic retrograde tracing data suggests this is possible (Rompani, Mullner et al. 2017). In contrast, the mouse SC is a much larger structure and ipsilateral RGCs are spread along a crescent spanning the anterior and medial borders. Furthermore, ipsilateral RGC terminals are organized into clusters, rather than a contiguous lamina, further reducing potential interactions. Thus, the probability of penetrations in early studies targeting these regions specifically may have been reduced, especially if the anteromedial regions was not intentionally sampled.

A second contributing factor could be derived from the classification strategy we utilized to determine binocular interactions. Previous studies in which abundant BN units were reported in the anterior SC of hamsters relied upon visual stimuli eliciting a response when presented through each eye (Tiao and Blakemore 1976). While we did find a subpopulation of BN neurons in the mouse SC, namely BN-S, the majority had more complex responses to presentation in multiple ocularity conditions. Indeed, the most numerous subtype we found, BN-E, only exhibit visual responsiveness when stimuli are presented to both eyes at the same time. It is likely that these units would not have been detected in previous studies, since they do not exhibit responses when stimuli are presented monocularly. And, BN-IbI and BN-IbC subtypes described here could be difficult to isolate if the opposing eye was not completely occluded during recording sessions. Of note, the responses we observed we elicited in the anesthetized state. Given the robust differences in visual tuning in the awake state (De Franceschi

and Solomon 2018), it will be interesting to determine if BN responses are similarly modulated.

Subtypes of BN neurons in the SC

A surprising result from these studies is the diversity of BN subtypes identified. Importantly, similar complements of BN responses were recently reported in the mouse dLGN (Huh, Abdelaal et al. 2020), suggesting that these modes of modulation may represent a common group of BN neurons in the mouse visual system. Interestingly, while most neurons in that study were exclusively driven monocularly, neurons similar to the BN-E subtype identified here comprised a substantial proportion of the thalamocortical population. And, neurons that exhibited responses in monocular conditions, but were suppressed under binocular conditions were also found (Huh, Abdelaal et al. 2020), similar to the BN-IbI and BN-IbC subtypes described here.

The identification of multiple subtypes of BN neurons in the SC begs the question of how these tuning properties arise. As mentioned above, the mouse SC receives inputs from both the ipsilateral and contralateral eye. Thus, an attractive hypothesis is that BN-S units derive their responsiveness from direct innervation by these two populations. And, BN-E tuning could be similarly derived, although inputs from each individual eye drive sub-threshold responses, perhaps due to the sparsity or distal localization of contacts onto the dendritic trees of SC neurons (Spruston 2008). More complex tuning properties, such as in BN-IbI and BN-IbC neurons, could arise through feed-forward inhibition from ipsilateral and contralateral RGCs via local interneurons.

In addition to RGCs, the SC receives visual input from multiple other regions that could relay binocular visual information. For instance, V1 projects topographically to the SC and in alignment with the retinocollicular map, providing one potential source of binocular input. However, studies have shown that binocular integration in the dLGN is independent of cortical feedback (Howarth, Walmsley et al. 2014, Jaepel, Hubener et al. 2017). Intriguingly, binocular responses are prevalent in the frog tectum, which arise not from direct ipsilateral RGC inputs, but rather indirectly from the nucleus isthmi (Udin 2012). The mammalian homologue of the nucleus isthmi, the parabigeminal nucleus, also projects to the SC and could convey binocular information. Future studies leveraging eye- or region-specific manipulations of activity are needed to resolve these possible circuit mechanisms.

Orientation and direction tuning of BN neurons

Since we utilized oriented drifting gratings as our stimulus to drive visual responses in all ocularity conditions, we were also able to interrogate the orientation- and direction-selectivity of BN subtypes. Interestingly, we found that substantial proportions of all four BN subtypes were classified as OS, suggesting the subtypes defined by ocularity may be able to be further subdivided based on their tuning preference.

One interesting finding here was that both MN and BN subtypes prefer closely related orientations of movement, with a predominant preference for directions between -90° and -30°. This suggests that neurons in the anteromedial SC tend to prefer vertical and leftward angled oblique orientations. These data are consistent with the concept

that relatively large areas of the SC exhibit similar tuning preferences (Feinberg and Meister 2015). Indeed, similar orientation preferences in the anteromedial SC were reported previously (Ahmadlou and Heimel 2015). The ethological relevance of such organization overall or specifically in the binocular region of the SC remains unclear. Previous work suggests that bilateral differences in direction-selectivity in the SC could be related to optic flow of the moving animal (de Malmazet, Kuhn et al. 2018), which could in turn help mediate specific behavioral repertoires executed by the SC.

Consistent with previous studies (Ito, Feldheim et al. 2017) most of the OS units we isolated were non-linear as defined by the F_1/F_0 ratio. Interestingly, BN units were more linear (higher F_1/F_0 ratio) compared to MN units. Specifically, BN-IbI and BN-IbC subtypes tended to have a more linear spatial summation of stimuli. Previously, the F_1/F_0 ratio has been used to differentiate simple versus complex cells in the cortex (Skottun, De Valois et al. 1991). This suggests that since BN-IbI and BN-IbC are more linear there is a possibility they have more simple-like receptive fields with non-overlapping ON and OFF subfields. Unfortunately, we did not map respective field substructure in this study, but it would be interesting to explore.

In subtypes where more than one eye was responsive (MN-C, MN-I and BN-S) we determined if visual response properties of OS neurons were similar across ocularities. When comparing gOSI, preferred direction, spatial frequency and linearity, MN-C cells were very consistent across ocularities. The trend here revealed that the CO and BO conditions had very similar responses. Interestingly, in the MN-I and BN-S conditions, this is less so. Overall, the IO condition did not correlate well with the BO or CO conditions. This may suggest that input from contralateral RGCs may contribute

more to visual processing properties and ipsilateral input less so. This may be due to a combination of fewer and/or weaker ipsilateral inputs to the anteromedial SC compared to contralateral inputs. Previous studies have shown that by P15, ipsilateral RGCs extend more widely throughout the rostrocaudal axis, but had fewer arbors compared to contralateral RGCs (Dhande, Hua et al. 2011).

In contrast to previous work, we did not encounter substantial numbers of DS units in this study. This may be due to the method of recording, since the majority of DS units in the SC are localized to the superficial-most SC (Inayat, Barchini et al. 2015), while our electrode penetrations were typically deeper. Of note, at least one DS unit was identified in each BN subtype, while none of the MN subtypes we encountered exhibited direction-selectivity. Again, this suggests that the ocularity-defined subtypes described here may be comprised of more specifically tuned subtypes. And, importantly, the directional preferences we found here are consistent with those previously reported for the anteromedial portion of the SC (de Malmazet, Kuhn et al. 2018).

Conclusion

Here, we report the surprising prevalence of BN neurons in the mouse SC, which are comprised of at least four subtypes based on their differential responses to ocularity-specific visual stimuli. Interestingly, these four subtypes may be comprised of even more specified cell types, as we uncovered both orientation- and direction-selectivity in each. And, these tuning properties were distinct from MN neighbors in the anteromedial SC, suggesting a potential segregation of functional purpose in extracting

information from the visual scene and/or translating into SC-regulated behavioral responses.

Figure Legends

Figure 1. Experimental design to identify binocularly-modulated neurons in the mouse SC. A) Schematic of presentation of drifting square waves visual stimuli to an anesthesized animal. B) A 16-channel silicone probe (NeuroNexus) was placed in the anteromedial region of the superficial SC. White arrow indicate electrode tract. C) Animals were exposed to visual stimuli in three ocularity conditions: both eyes open (BO), eye contralateral to the recording site open (CO) and ipsilateral eye open (IO). D) Table representing the putative monocular (MN) and binocular (BN) cell subtypes.

Figure 2. Peristimulus spike time histograms (PSTH) of MN cells. A) Representative PSTH of Contra-driven (MN-C) cell. MN-C cells are defined by visual responsiveness in the BO and CO conditions, but not the IO condition. A cell was determined as visually responsive if the peak firing rate was > 3 SD above the spontaneous rate (top row) in ≥ 50% of the trials (bottom row). B) Representative plot of peak firing rate across all ocularity conditions and stimuli trials. C) Peak firing rate was significantly correlated when comparing the BO and CO responses. D, E) Representative PSTH and peak firing rates of Ipsi-driven (MN-I) cell. MN-I are defined by visual responsiveness in the BO and

IO conditions, but not the CO condition. F) Peak firing rate was not correlated between the BO and IO conditions for MN-I cells.

Figure 3. PSTHs of BN subtypes. A) Representative PSTH of a BN Simple (BN-S) cell. BN-S cells were visually responsive in all ocularity conditions (BO, CO and IO). B) Peak firing rate across ocularity conditions in BN-S cells C, D) Representative PSTH of an BN Emergent (BN-E) cells. BN-E were only visually responsive when both eyes were open. E, F) Representative PSTH of an BN Inhibited by Ipsi (BN-IbI) cell. BN-IbI cells were only visually responsive in the CO condition. BO and IO did not elicit a response. G) Representative PSTH of an BN Inhibited by Contra (BN-IbC) cell. BN-IbC were only responsive in the IO condition. BO and CO did not elicit a response.

Figure 4. Proportions and firing rates of MN and BN subtypes. A) In the anteromedial SC, both MN and BN neurons were identified (middle chart). As expected the majority of MN cells are contra-driven (MN-C) with fewer being Iipsi-driven (MN-I) (right chart). The left chart shows the proportions of each of the four BN subtypes. B) There were no differences in either baseline or peak firing rates between visually responsive MN and BN cells. C) There were no differences in baseline or peak firing rates between visually responsive cell subtypes. In all comparisons, the peak firing rate was significantly higher than respective baseline firing rate (data not indicated on B and C).

Figure 5. Orientation selectivity of MN and BN cell. Quantification of gOSI values A) between MN and BN groups and B) between subtypes. Relative percent of visually

responsive neurons that were orientation selective (OS) in C) MN and BN groups and D) between subtypes. gOSI correlations in the E) MN-C cells between CO and BO and FMN-I between IO and BO and G,H) BN-S between the ocularity conditions.

Figure 6. Tuning properties of MN and BN OS neurons. A-F) Representative polar plots of A) MN-C, B) MN-I, C) BN-S, D) BN-E, E) BN-IbI and F) BN-IbC subtypes. Solid lines refer to the BO condition, long dashed lines represent the CO open condition and short dashed lines represent the IO condition in each subtype. G) Change in preferred direction between eyes in conditions where two eyes were responsive (MN-C, MN-I and BN-S) H) Cumulative percent of preferred orientation of OS neurons in each subtype I) Quantification of tuning width (deg) between subtypes.

Figure 7. Spatial frequency of MN and BN OS neurons. A) Cumulative percent of preferred spatial frequency (SF) in each subtype. B) Quantification of SF bandwidth (octaves) between subtypes. C) Quantification of change in octaves between eyes in conditions where two eyes were responsive.

Figure 8. Linearity of MN and BN OS neurons. A-B) Quantification of F_1/F_0 ratio in A) MN and BN groups and B) between MN- and BN-modulated neuronal subtypes. C) Relative percent of OS units that are linear (>1.0) and non-linear (<1.0) in each subtype. D) Quantification of change in F_1/F_0 ratio between eyes in conditions where two eyes were responsive (MN-C, MN-I and BN-S).

Figure 9. Direction selectivity in MN and BN neurons. A-B) Quantification of gDSI A) in MN and BN groups and B) between MN- and BN-modulated subtypes. C-F) Representative polar plots of DS neurons in C) BN-S, D) BN-E, E) BN-IbI and F) BN-IbC.

References

Ahmadlou, M. and J. A. Heimel (2015). "Preference for concentric orientations in the mouse superior colliculus." Nat Commun **6**: 6773.

Basso, M. A. and P. J. May (2017). "Circuits for Action and Cognition: A View from the Superior Colliculus." Annu Rev Vis Sci **3**: 197-226.

Berman, N., C. Blakemore and M. Cynader (1975). "Binocular interaction in the cat's superior colliculus." J Physiol **246**(3): 595-615.

Chalupa, L. M. and R. W. Rhoades (1977). "Responses of visual, somatosensory, and auditory neurones in the golden hamster's superior colliculus." J Physiol **270**(3): 595-626.

Chaturvedi, V. and J. A. van Gisbergen (1999). "Perturbation of combined saccade-vergence movements by microstimulation in monkey superior colliculus." J Neurophysiol **81**(5): 2279-2296.

Chaturvedi, V. and J. A. Van Gisbergen (2000). "Stimulation in the rostral pole of monkey superior colliculus: effects on vergence eye movements." Exp Brain Res **132**(1): 72-78.

De Franceschi, G. and S. G. Solomon (2018). "Visual response properties of neurons in the superficial layers of the superior colliculus of awake mouse." J Physiol **596**(24): 6307-6332.

de Malmazet, D., N. K. Kuhn and K. Farrow (2018). "Retinotopic Separation of Nasal and Temporal Motion Selectivity in the Mouse Superior Colliculus." Curr Biol **28**(18): 2961-2969 e2964.

Dhande, O. S., E. W. Hua, E. Guh, J. Yeh, S. Bhatt, Y. Zhang, E. S. Ruthazer, M. B. Feller and M. C. Crair (2011). "Development of single retinofugal axon arbors in normal and beta2 knock-out mice." J Neurosci **31**(9): 3384-3399.

Dias, E. C., C. E. Rocha-Miranda, R. F. Bernardes and S. L. Schmidt (1991). "Disparity selective units in the superior colliculus of the opossum." Exp Brain Res **87**(3): 546-552.

Drager, U. C. and D. H. Hubel (1975). "Physiology of visual cells in mouse superior colliculus and correlation with somatosensory and auditory input." Nature **253**(5488): 203-204.

Ellis, E. M., G. Gauvain, B. Sivyer and G. J. Murphy (2016). "Shared and distinct retinal input to the mouse superior colliculus and dorsal lateral geniculate nucleus." J Neurophysiol **116**(2): 602-610.

Feinberg, E. H. and M. Meister (2015). "Orientation columns in the mouse superior colliculus." Nature **519**(7542): 229-232.

Goldberg, M. E. and R. H. Wurtz (1972). "Activity of superior colliculus in behaving monkey. I. Visual receptive fields of single neurons." J Neurophysiol **35**(4): 542-559.

Grieve, K. L. (2005). "Binocular visual responses in cells of the rat dLGN." J Physiol **566**(Pt 1): 119-124.

Gu, Y. and J. Cang (2016). "Binocular matching of thalamocortical and intracortical circuits in the mouse visual cortex." Elife **5**.

Haustead, D. J., S. S. Lukehurst, G. T. Clutton, C. A. Bartlett, S. A. Dunlop, C. A. Arrese, R. M. Sherrard and J. Rodger (2008). "Functional topography and integration of the contralateral and ipsilateral retinocollicular projections of ephrin-A-/- mice." J Neurosci **28**(29): 7376-7386.

Howarth, M., L. Walmsley and T. M. Brown (2014). "Binocular integration in the mouse lateral geniculate nuclei." Curr Biol **24**(11): 1241-1247.

Huh, C. Y. L., K. Abdelaal, K. J. Salinas, D. Gu, J. Zeitoun, D. X. Figueroa Velez, J. P. Peach, C. C. Fowlkes and S. P. Gandhi (2020). "Long-term Monocular Deprivation during Juvenile Critical Period Disrupts Binocular Integration in Mouse Visual Thalamus." J Neurosci **40**(3): 585-604.

Inayat, S., J. Barchini, H. Chen, L. Feng, X. Liu and J. Cang (2015). "Neurons in the most superficial lamina of the mouse superior colliculus are highly selective for stimulus direction." J Neurosci **35**(20): 7992-8003.

Ito, S., D. A. Feldheim and A. M. Litke (2017). "Segregation of Visual Response Properties in the Mouse Superior Colliculus and Their Modulation during Locomotion." J Neurosci **37**(35): 8428-8443.

Jaepel, J., M. Hubener, T. Bonhoeffer and T. Rose (2017). "Lateral geniculate neurons projecting to primary visual cortex show ocular dominance plasticity in adult mice." Nat Neurosci **20**(12): 1708-1714.

Kay, R. B., N. A. Gabreski and J. W. Triplett (2018). "Visual subcircuit-specific dysfunction and input-specific mispatterning in the superior colliculus of fragile X mice." J Neurodev Disord **10**(1): 23.

Kay, R. B. and J. W. Triplett (2017). "Visual Neurons in the Superior Colliculus Innervated by Islet2(+) or Islet2(-) Retinal Ganglion Cells Display Distinct Tuning Properties." Front Neural Circuits **11**: 73.

Mimeault, D., V. Paquet, S. Molotchnikoff, F. Lepore and J. P. Guillemot (2004). "Disparity sensitivity in the superior colliculus of the cat." Brain Res **1010**(1-2): 87-94.

Morgan, J. L., D. R. Berger, A. W. Wetzel and J. W. Lichtman (2016). "The Fuzzy Logic of Network Connectivity in Mouse Visual Thalamus." Cell **165**(1): 192-206.

Niell, C. M. and M. P. Stryker (2008). "Highly selective receptive fields in mouse visual cortex." J Neurosci **28**(30): 7520-7536.

Rompani, S. B., F. E. Mullner, A. Wanner, C. Zhang, C. N. Roth, K. Yonehara and B. Roska (2017). "Different Modes of Visual Integration in the Lateral Geniculate Nucleus Revealed by Single-Cell-Initiated Transsynaptic Tracing." Neuron **93**(6): 1519.

Scholl, B., J. Burge and N. J. Priebe (2013). "Binocular integration and disparity selectivity in mouse primary visual cortex." J Neurophysiol **109**(12): 3013-3024.

Shi, X., J. Barchini, H. A. Ledesma, D. Koren, Y. Jin, X. Liu, W. Wei and J. Cang (2017). "Retinal origin of direction selectivity in the superior colliculus." Nat Neurosci **20**(4): 550-558.

Skottun, B. C., R. L. De Valois, D. H. Grosof, J. A. Movshon, D. G. Albrecht and A. B. Bonds (1991). "Classifying simple and complex cells on the basis of response modulation." Vision Res **31**(7-8): 1079-1086.

Spruston, N. (2008). "Pyramidal neurons: dendritic structure and synaptic integration." Nat Rev Neurosci **9**(3): 206-221.

Suzuki, S., Y. Suzuki and K. Ohtsuka (2004). "Convergence eye movements evoked by microstimulation of the rostral superior colliculus in the cat." Neurosci Res **49**(1): 39-45.

Tiao, Y. C. and C. Blakemore (1976). "Functional organization in the superior colliculus of the golden hamster." J Comp Neurol **168**(4): 483-503.

Udin, S. B. (2012). "Binocular maps in Xenopus tectum: Visual experience and the development of isthmotectal topography." Dev Neurobiol **72**(4): 564-574.

Van Horn, M. R., D. M. Waitzman and K. E. Cullen (2013). "Vergence neurons identified in the rostral superior colliculus code smooth eye movements in 3D space." J Neurosci **33**(17): 7274-7284.

Wang, L., R. Sarnaik, K. Rangarajan, X. Liu and J. Cang (2010). "Visual receptive field properties of neurons in the superficial superior colliculus of the mouse." J Neurosci **30**(49): 16573-16584.

Zeater, N., S. K. Cheong, S. G. Solomon, B. Dreher and P. R. Martin (2015). "Binocular Visual Responses in the Primate Lateral Geniculate Nucleus." Curr Biol **25**(24): 3190-3195.

Zhao, X., M. Liu and J. Cang (2013). "Sublinear binocular integration preserves orientation selectivity in mouse visual cortex." Nat Commun **4**: 2088.

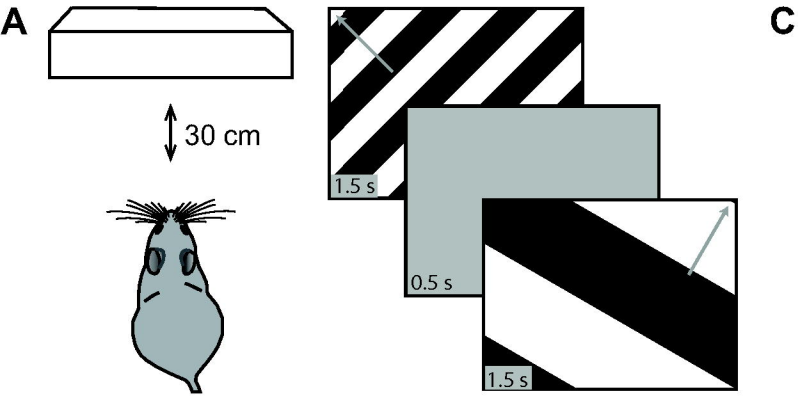

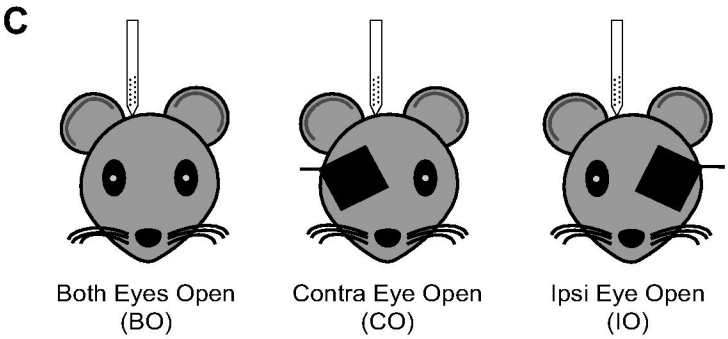

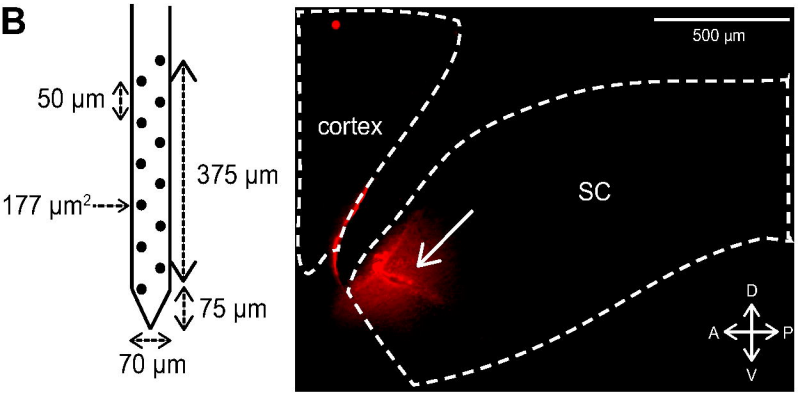

D

Putative Cell Types

		BO	CO	IO
Monocular	Contra-driven	+	+	-
	Ipsi-driven	+	-	+
Binocular	Simple	+	+	+
	Emergent	+	-	-
	Inh by Ipsi	-	+	-
	Inh by Contra	-	-	+
	Cross-Inhibited	-	+	+

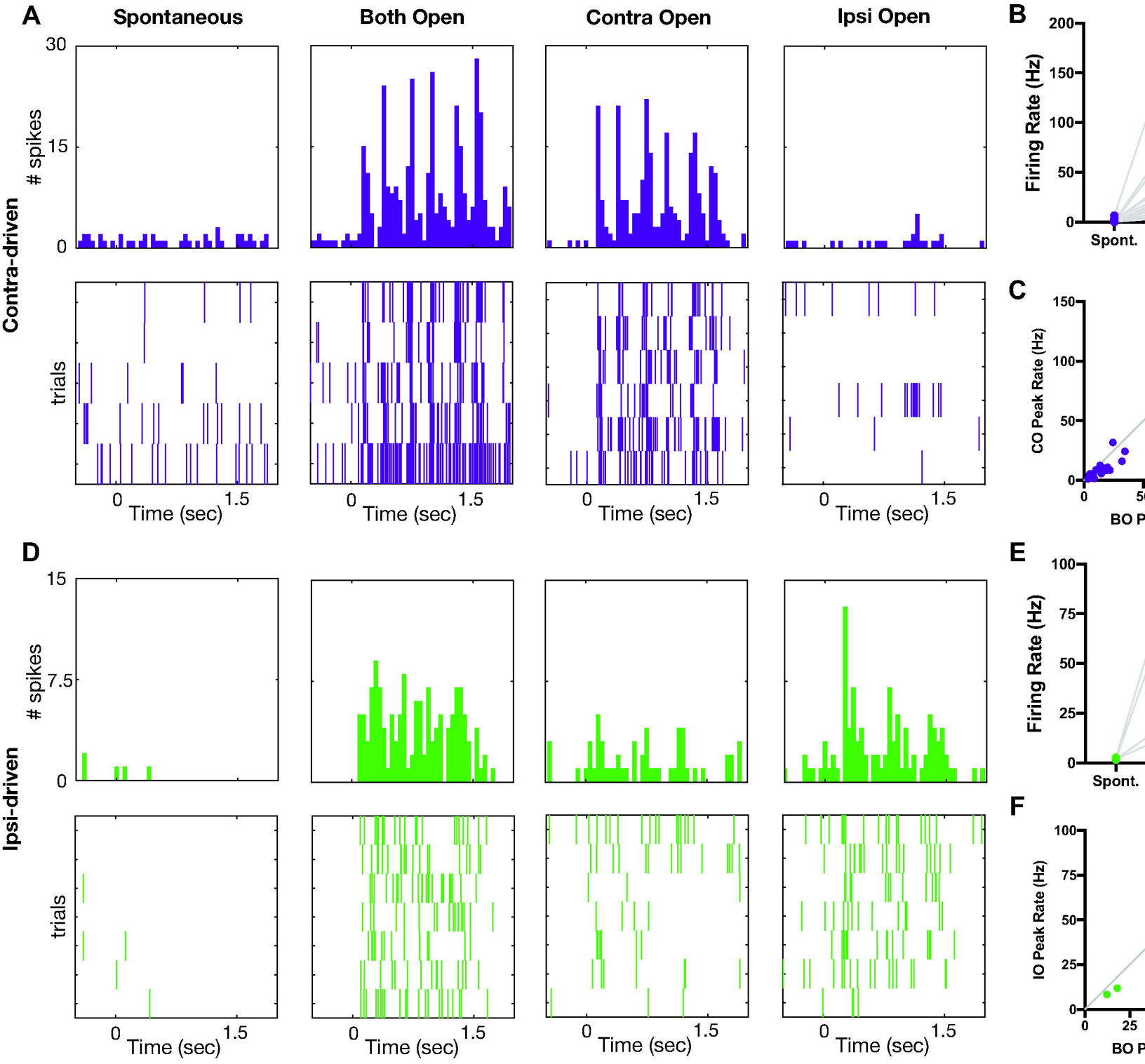
A
Spontaneous
Both Open
Contra Open
Ipsi Open
Contra-driven
spikes
trials
Time (sec)
B
Firing Rate (Hz)
Spont.
C
CO Peak Rate (Hz)
D
Ipsi-driven
E
F
IO Peak Rate (Hz)

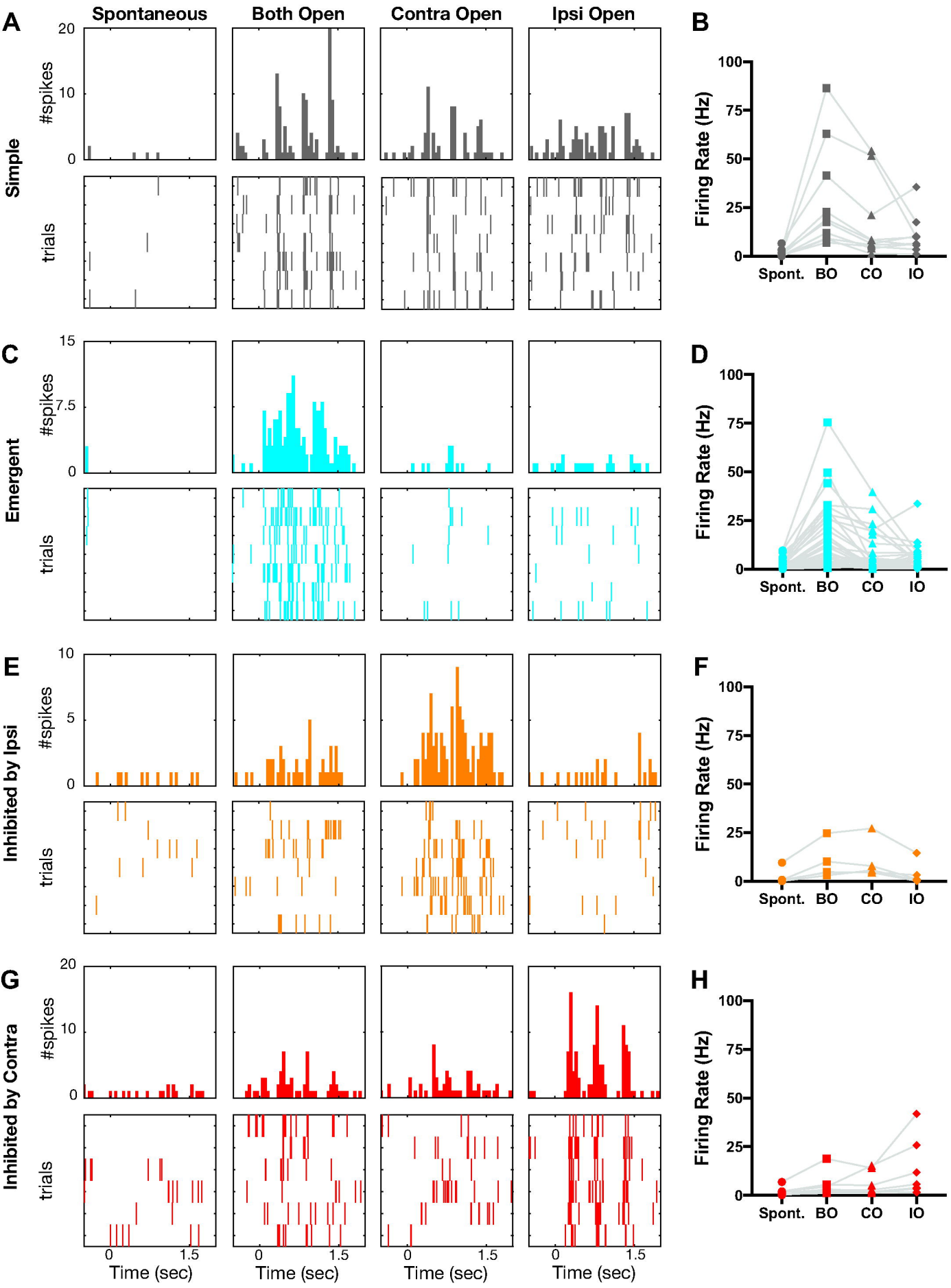
A
Spontaneous
Both Open
Contra Open
Ipsi Open
Simple
#spikes
trials
B
Firing Rate (Hz)
Spont.
BO
CO
IO
C
Emergent
D
E
Inhibited by Ipsi
F
G
Inhibited by Contra
H
Time (sec)

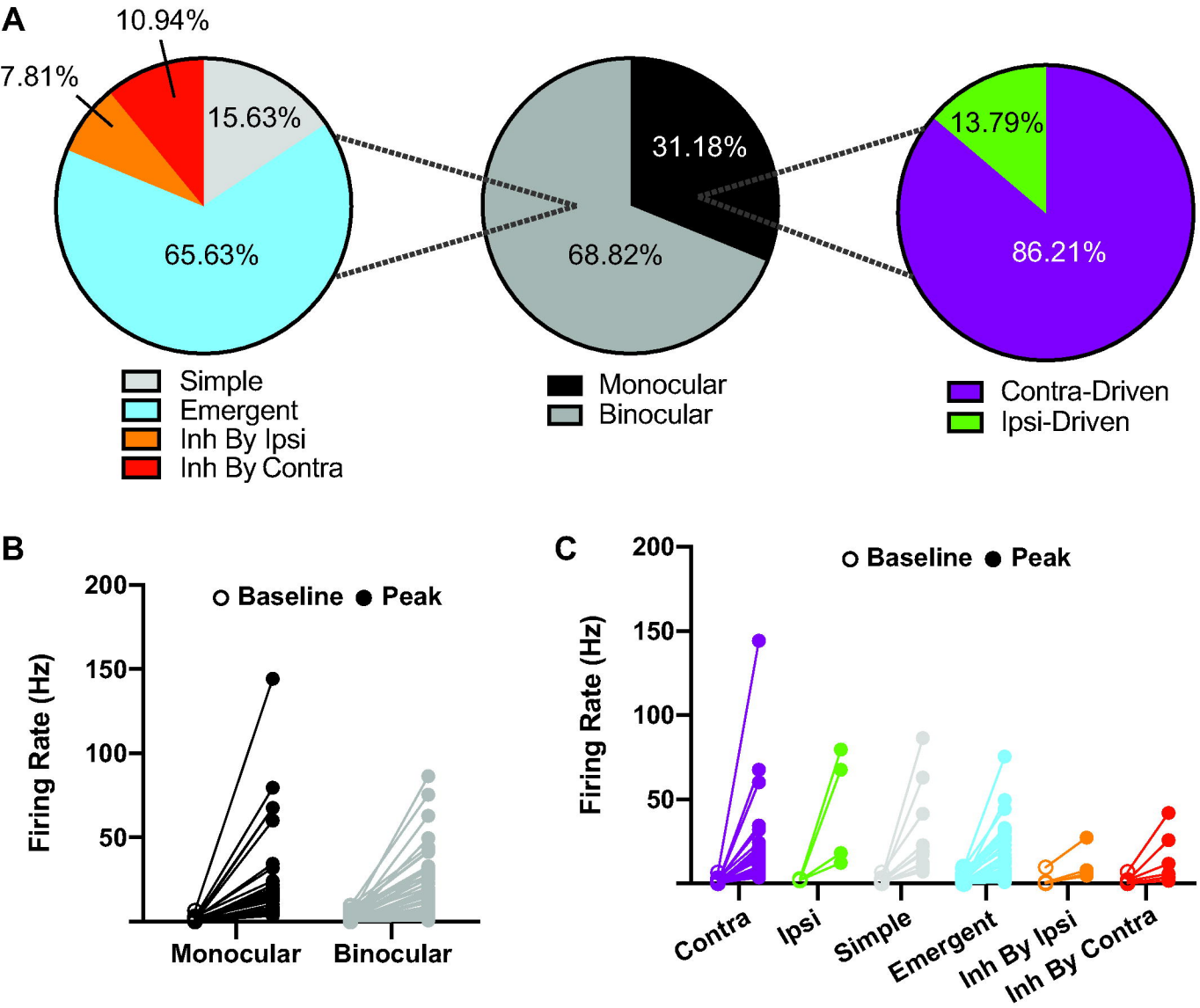
A
10.94%
7.81%
15.63%
65.63%
31.18%
68.82%
13.79%
86.21%
Simple
Emergent
Inh By Ipsi
Inh By Contra
Monocular
Binocular
Contra-Driven
Ipsi-Driven
B
Baseline
Peak
Firing Rate (Hz)
200
150
100
50
Monocular
Binocular
C
Baseline
Peak
Firing Rate (Hz)
200
150
100
50
Contra
Ipsi
Simple
Emergent
Inh By Ipsi
Inh By Contra

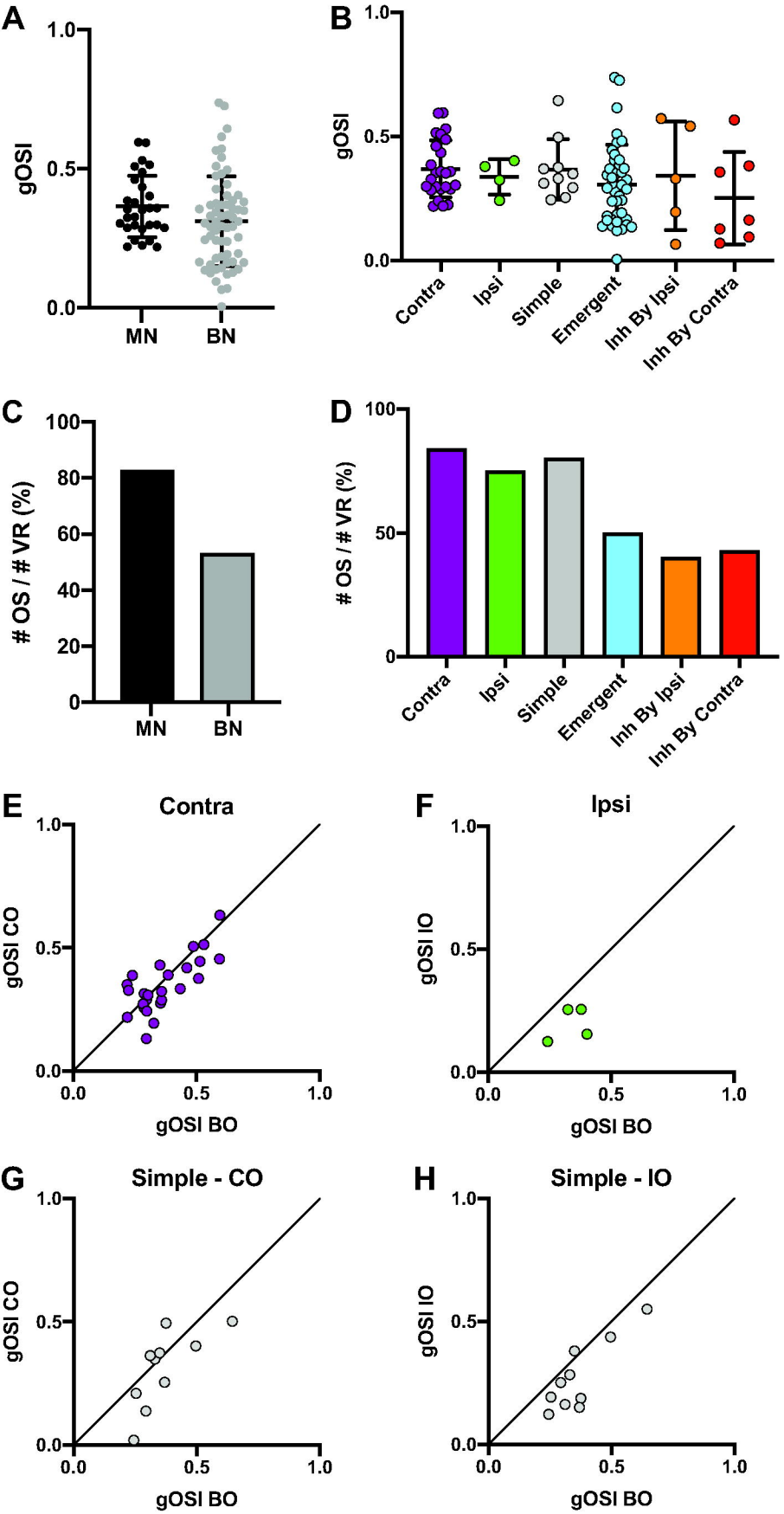
A
gOSI
1.0
0.5
0.0
MN
BN
B
gOSI
1.0
0.5
0.0
Contra
Ipsi
Simple
Emergent
Inh By Ipsi
Inh By Contra
C
OS / # VR (%)
100
80
60
40
20
0
MN
BN
D
OS / # VR (%)
100
50
0
Contra
Ipsi
Simple
Emergent
Inh By Ipsi
Inh By Contra
E
Contra
gOSI CO
gOSI BO
F
Ipsi
gOSI IO
gOSI BO
G
Simple - CO
gOSI CO
gOSI BO
H
Simple - IO
gOSI IO
gOSI BO

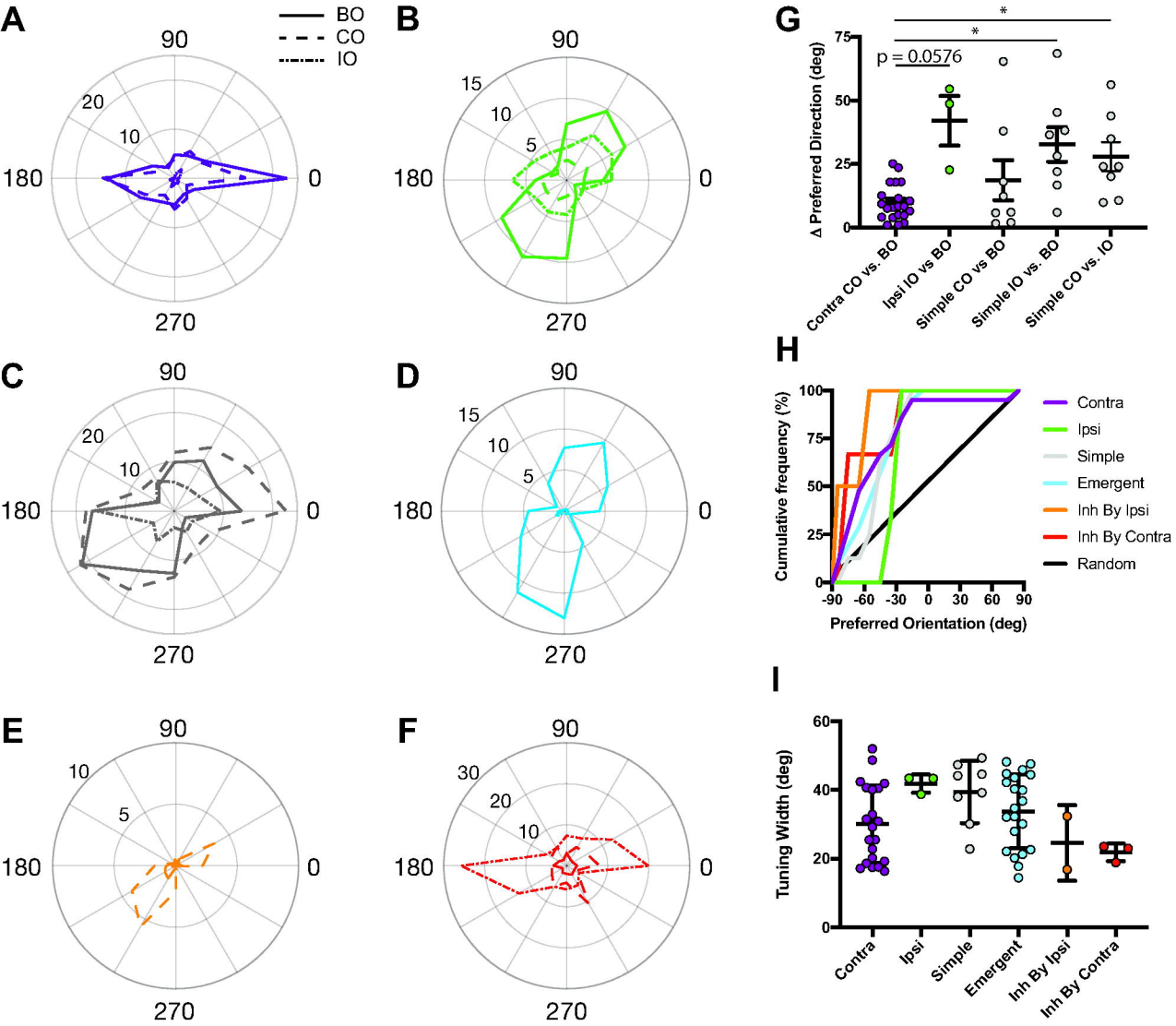
A
BO
CO
IO
90
180
0
270
20
10
B
15
10
5
C
D
E
10
5
F
30
20
10
G
Δ Preferred Direction (deg)
p = 0.0576
*
*
Contra CO vs. BO
Ipsi IO vs BO
Simple CO vs BO
Simple IO vs. BO
Simple CO vs. IO
H
Cumulative frequency (%)
Preferred Orientation (deg)
Contra
Ipsi
Simple
Emergent
Inh By Ipsi
Inh By Contra
Random
I
Tuning Width (deg)
Contra
Ipsi
Simple
Emergent
Inh By Ipsi
Inh By Contra

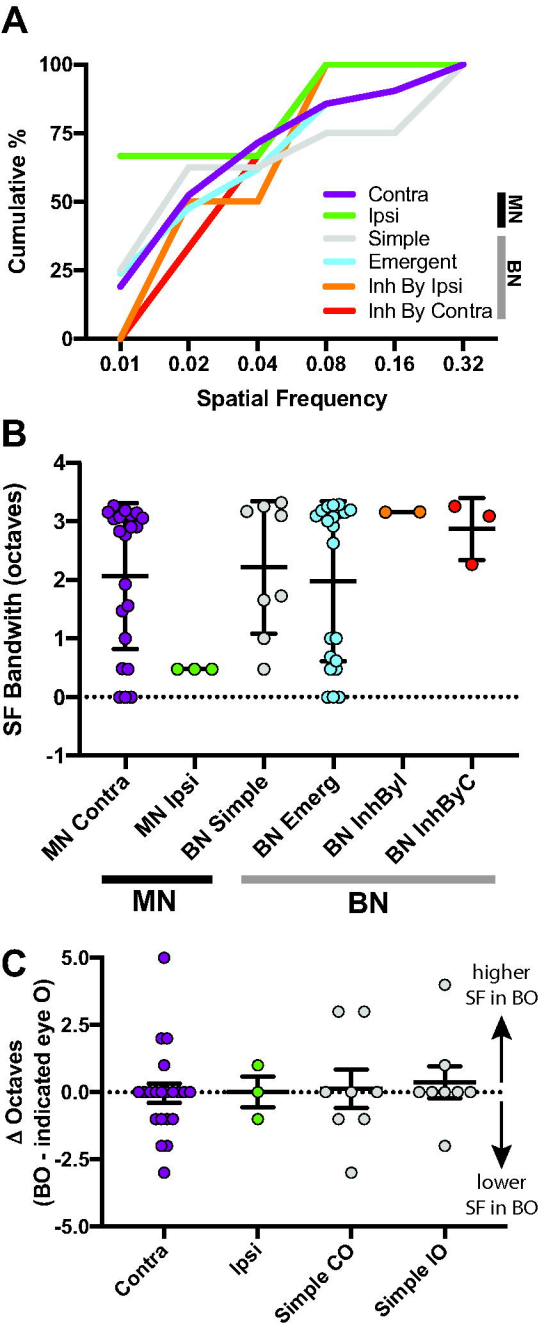
A
Cumulative %
100
75
50
25
0
0.01
0.02
0.04
0.08
0.16
0.32
Spatial Frequency
Contra
Ipsi
Simple
Emergent
Inh By Ipsi
Inh By Contra
MN
BN
B
SF Bandwith (octaves)
4
3
2
1
0
-1
MN Contra
MN Ipsi
BN Simple
BN Emerg
BN InhByI
BN InhByC
MN
BN
C
Δ Octaves
(BO - indicated eye O)
5.0
2.5
0.0
-2.5
-5.0
higher
SF in BO
lower
SF in BO
Contra
Ipsi
Simple CO
Simple IO

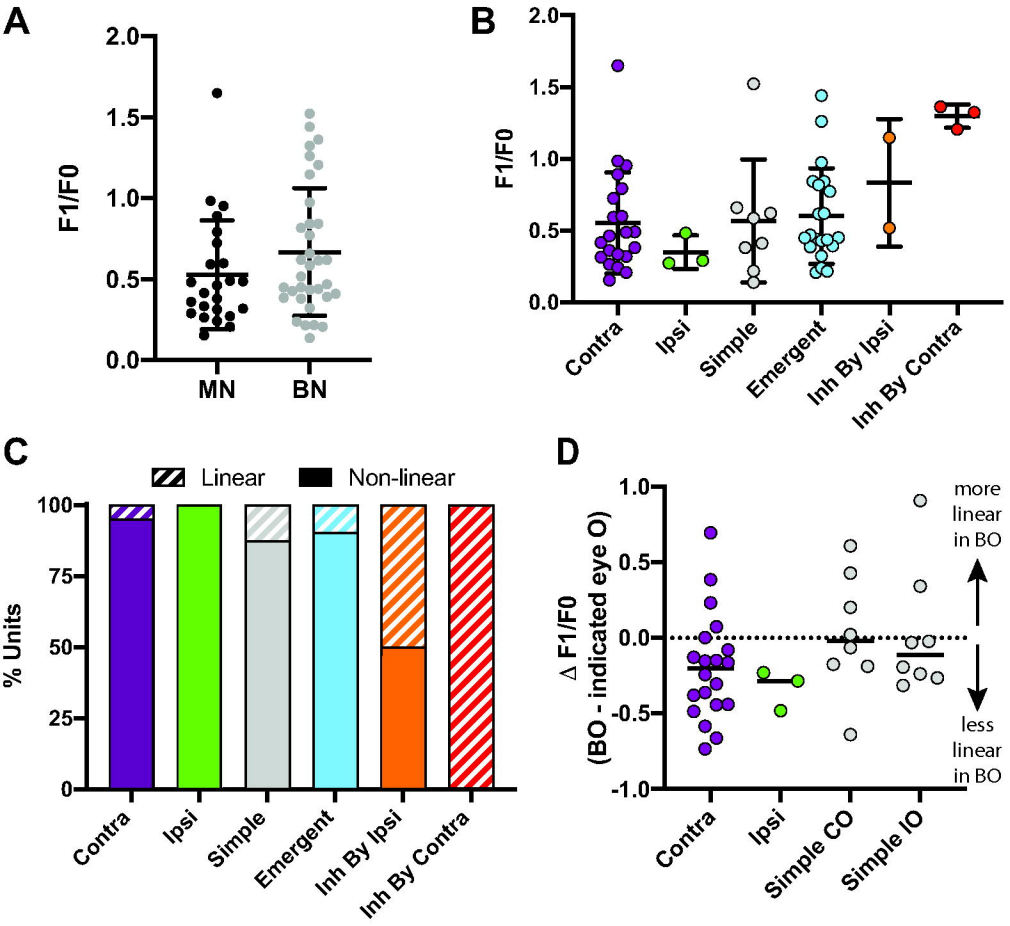
A
F1/F0
2.0
1.5
1.0
0.5
0.0
MN
BN
B
F1/F0
2.0
1.5
1.0
0.5
0.0
Contra
Ipsi
Simple
Emergent
Inh By Ipsi
Inh By Contra
C
Linear
Non-linear
% Units
100
75
50
25
0
Contra
Ipsi
Simple
Emergent
Inh By Ipsi
Inh By Contra
D
Δ F1/F0
(BO - indicated eye O)
1.0
0.5
0.0
-0.5
-1.0
more
linear
in BO
less
linear
in BO
Contra
Ipsi
Simple CO
Simple IO

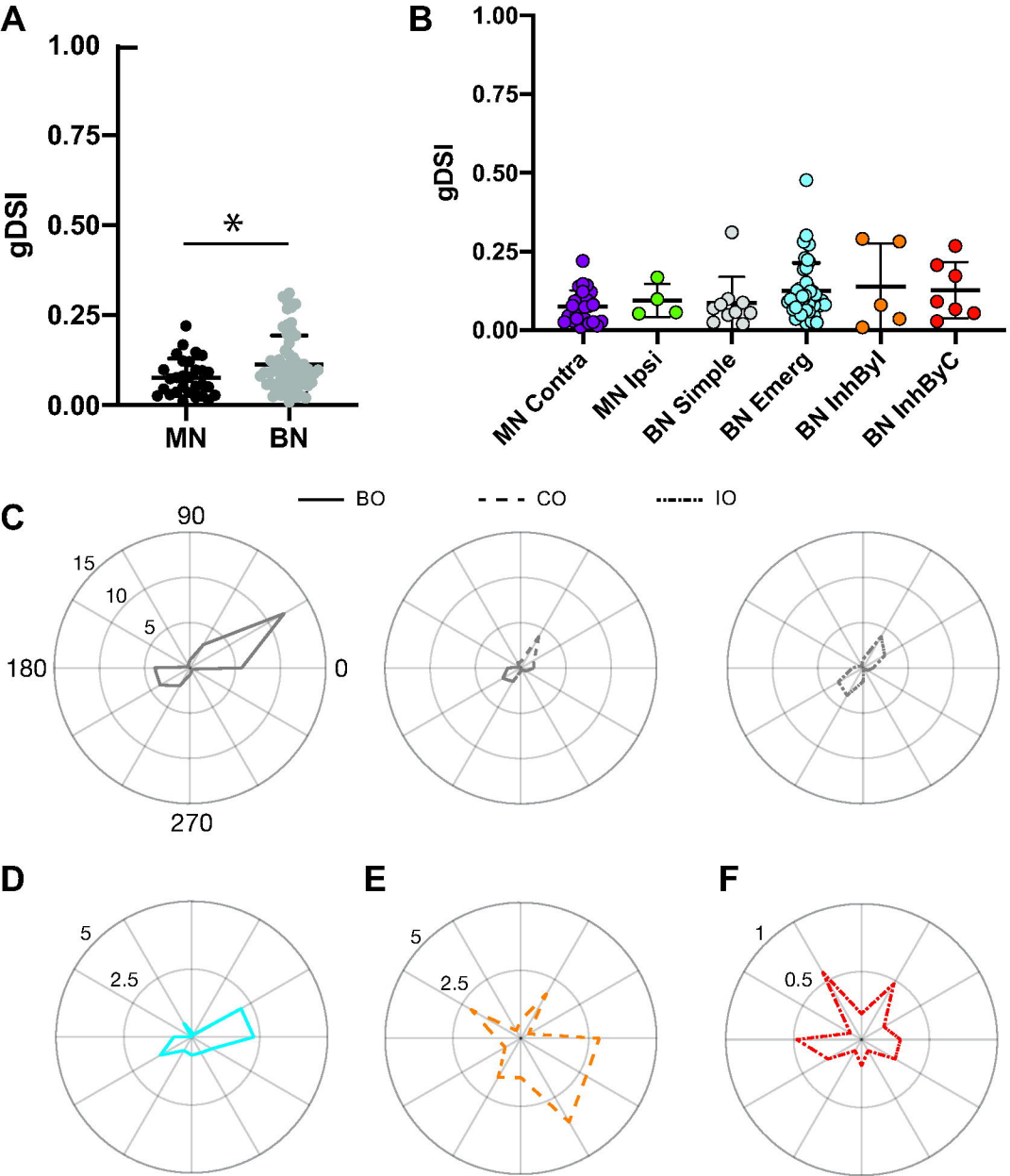
A
1.00
0.75
0.50
0.25
0.00
gDSI
*
MN
BN
B
1.00
0.75
0.50
0.25
0.00
gDSI
MN Contra
MN Ipsi
BN Simple
BN Emerg
BN InhByI
BN InhByC
C
BO
CO
IO
90
15
10
5
180
0
270
D
5
2.5
E
5
2.5
F
1
0.5